# BOXES STRUCTURE CONSTRUCTION AROUND THE CLUSTERS OF VORTEX ELEMENTS TO REDUCE THE COMPUTATIONAL COST OF A LAGRANGIAN VORTEX METHOD WITH ROUGHNESS MODEL

**Crystianne Lilian de Andrade**, crystiannelilian@yahoo.com.br
**Luiz Antonio Alcântara Pereira**, luizantp@unifei.edu.br
Mechanical Engineering Institute, Federal University of Itajubá (UNIFEI), Itajubá, Brazil

**Alex Mendonça Bimbato**, alexbimbato@feg.unesp.br
Department of Energy, São Paulo State University (UNESP), Guaratinguetá, Brazil

***Abstract.*** *The aim of this paper is to present a numerical procedure that accelerates the second-order velocity structure function model calculation incorporated into the Lagrangian Vortex Method with turbulence modeling. In the present study, the local turbulence effects are considered during the vorticity diffusion process; as consequence a connection between the larger scales and the smaller ones is made by eddy viscosity. The eddy viscosity computation is necessary for each Lamb vortex element that constructs the Kármán vortex street; it is also the key to take into account the roughness effects. A boxes structure is used to identify clusters of vortex elements confined in different regions of the fluid domain. The boxes structure establishes interaction lists between vortex elements in a lower computational cost. The CPU time, necessary to compute the eddy viscosity is considerably reduced.*

***Keywords:*** *two-dimensional roughness model; panel methods, reduction of the computational cost; aerodynamics of bluff body.*

## 1. INTRODUCTION

Unsteady vorticity-dominated flows are of great interest in many fluid mechanics problems. In this context, the Lagrangian Vortex Methods can be used to approximate time-dependent incompressible flows. In this kind of flow most of the vorticity is confined to a relatively small portion of the flow, and then a purely Lagrangian Vortex Method based on following the vorticity by using vortex elements does not depend on the construction of a good-quality mesh on the domain of computation (the Eulerian and grid-dependent methods suffer inevitably from numerical diffusion). The main advantages of a Lagrangian Vortex Method are that vortex elements are placed only where vorticity is non-zero and the boundary conditions in the far field are automatically satisfied. Lagrangian vortex methods are especially useful to solve flows which are dominated by localized vorticity distributions, e.g., shear flows, wakes, and jets (Kamemoto, 2004).

The present paper attempts to control the flow around a circular cylinder of diameter d through the implementation of surface roughness model around the exterior of the body. The mechanism of vortex shedding of rough stationary cylinder in the subcritical flow regime ($Re=10^5$) is simulated using a two-dimensional Lagrangian Vortex Method. The local turbulence effects are taking into account through a second order velocity structure function model adapted to a Lagrangian Vortex Method (Alcântara Pereira et al., 2002). The intensity of newly generated Lamb vortex elements (Kundu, 1990) from the body surface is in a physical sense affected for the local effects of size of uniformly distributed roughness elements, $\varepsilon/d$. Therefore, the mass and the global circulation are simultaneously conserved using a source panel method and generation of vortex elements along the body surface. The aerodynamic loads are calculated using an integral formulation derived from the pressure Poisson equation (Shintani & Akamatsu, 1994). The contribution of this paper is to accelerate the eddy viscosity computation through a new algorithm for the boxes structure construction aiming to divide the vortex elements into the groups across the fluid domain.

According to Bimbato (2012) a two-dimensional surface roughness model is more effective than a single two-dimensional turbulence model. His research indicated the potentialities of a two-dimensional Lagrangian vortex method with physical roughness model to predict the aerodynamics of bluff bodies with rough surface providing a good data base for further research using different Reynolds numbers associated with roughness size and distributions. Previous results from Guven et al. (1980) showed in a drag coefficient *versus* Reynolds diagram comparisons of different results, and they presented differences up to 60% for a given Reynolds number. These differences were attributed to some influencing factors, such as: aspect ratio, blockage ratio, turbulence level and the surface texture. The greater differences were observed in the supercritical flow regime which indicated the importance of the roughness models developing. The flow regimes cannot be characterized only by the Reynolds number based on the size of the roughness.

## 2. PROBLEM FORMULATION

Figure 1 illustrates the incompressible and two-dimensional flow around a circular cylinder, being the fluid Newtonian with constant kinematic viscosity, $\nu$. The uniform flow is represented by U and assumed from left to right. The fluid domain $\Omega$ is identified by the boundary $S=S_1 \cup S_2$, being $S_1$ the body surface and $S_2$ the far away boundary.

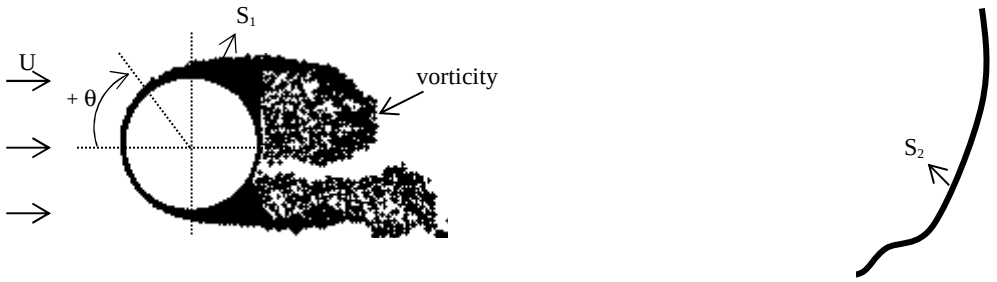


Figure 1. Unsteady viscous flow around a stationary circular cylinder.

The flow depicted above is governed by the continuity and the Navier-Stokes equations, which can be respectively written in the following forms:

$$\frac{\partial \overline{u}_i}{\partial x_i} = 0\,, \tag{1}$$

$$\frac{\partial \overline{u}_i}{\partial t} + \frac{\partial}{\partial x_j}\left(\overline{u}_i \overline{u}_j\right) = -\frac{1}{\rho}\frac{\partial \overline{p}}{\partial x_i} + 2\frac{\partial}{\partial x_j}\left[(\upsilon + \upsilon_t)\overline{S}_{ij}\right], \tag{2}$$

where $\overline{u}_i$ is the velocity filtered field, $\overline{p}$ is the pressure filtered field, $\rho$ is the density, $v$ is the molecular viscosity coefficient, $\upsilon_t$ is the eddy viscosity coefficient and $\overline{S}_{ij}$ is the deformation tensor of the filtered field (Smagorinsky, 1963).

The present methodology calculates the local spectrum at $K_c$ with a second-order velocity structure function, $\overline{F}_2$, of the filtered field ( velocities difference), such as (Alcântara Pereira et al., 2002):

$$\overline{F}_2\left(\boldsymbol{x}, \Delta^+, t\right) = \left\| \overline{\boldsymbol{u}}(\boldsymbol{x},t) - \overline{\boldsymbol{u}}(\boldsymbol{x}+\boldsymbol{r},t) \right\|^2_{|\boldsymbol{r}|=\Delta^+}\,. \tag{3}$$

From the Kolmogorov spectrum, the eddy viscosity can be written as a function of $\overline{F}_2$:

$$\upsilon_t\left(\boldsymbol{x}, \Delta^+, t\right) = 0.105 C_k^{-3/2} \Delta^+ \sqrt{\overline{F}_2\left(\boldsymbol{x}, \Delta^+, t\right)}\,, \tag{4}$$

where $C_k = 1.4$ is the Kolmogorov constant. In Eq. (3) is important to note that in three-dimensions the "average operator" is applied in the velocities $\boldsymbol{u}(\boldsymbol{x}+\boldsymbol{r},t)$ calculated under the surface of a sphere with center in $\boldsymbol{x}$ and radius $|\boldsymbol{r}|$. The present formulation analyses the vorticity dynamics in two-dimensions by taking the curl of the Navier-Stokes and, therefore, simulates numerically the phenomena that occur in the macro-scales by using a Lagrangian Vortex Method. Therefore, the phenomena that occur in the micro-scales should be taken into account through the eddy viscosity coefficient computation, see Eq. (4); the coefficient $v_t$ is modeled with the second-order velocity structure function, $\overline{F}_2$, of the filtered field, see Eq. (3), and must be computed to each vortex element during all steps of a typical numerical simulation. In two-dimensions $\boldsymbol{r}$ is the distance between each vortex element under analysis and other vortex elements strategically placed inside a circular crown. The center of each circular crown always coincides with the center of each vortex element, which is used to compute Eq. (4) (Alcântara Pereira et al. (2002) and Bimbato et al. (2013)).

.

## 3. NUMERICAL METHOD

The essence of the Lagrangian Vortex Method is to discretize the vorticity field using Lamb vortex elements in a manner that (Kundu, 1990):

$$\overline{\boldsymbol{\omega}}(\boldsymbol{x},t) = \sum_{k=1}^{NV} \frac{\Gamma_k}{\pi \sigma_{0_k}^2} exp\left(-\frac{|\boldsymbol{x}|^2}{\sigma_{0_k}^2}\right), \tag{5}$$

where $\overline{\boldsymbol{\omega}}$ ($\overline{\boldsymbol{\omega}} = \nabla \times \overline{\boldsymbol{u}}$) is the vorticity filtered field, $NV$ is the total number of vortex elements in the fluid domain, $\Gamma_k$ is the strength of the $k^{th}$ vortex element necessary to satisfy the no-slip condition on body surface and $\sigma_0$ is the Lamb vortex core given by (Bimbato, 2012):

$$\sigma_0 = 4.48364\sqrt{\frac{\Delta t}{Re}}\chi\,, \tag{6}$$

being $\chi$ a factor obtained through numerical experiences and crucial to determine the appropriate value of the Lamb vortex core. This approach considers the influence of source flat panels used to simulate the body surface through the impermeability condition (Katz and Plotkin, 1991). It is important to observe that each flat panel has a pivotal point necessary to simultaneously impose the no-slip and the impermeability conditions.

Presently, each nascent vortex element must be positioned at a shedding point near its respective pivotal point. Figure 2(a) shows one of the source flat panels used to represent the body surface; it is illustrated how the vorticity is generated on a smooth surface (note that $co$ is the pivotal point, $pshed'$ is the shedding point, $eps'$ is the distance between the pivotal point and the center of the vortex element and $\sigma_0$ is the Lamb vortex core).

In order to determine the turbulent activity around the shedding point of a $i^{th}$ panel are defined in the Fig. 2(b) the $pshed_i'$ point and the semicircle with radius $\|\boldsymbol{b}\| = 2\varepsilon - eps'$ ($\varepsilon = \varepsilon^*/d^*$) centered on shedding point $i$. A point set, called rough points, are distributed on the semicircle. The average speed differences necessary to determine the second-order velocity structure function of the filtered field (see Eq. (3)) are computed between the center of the semicircle ($pshed_i'$ point) and the rough points according to:

$$\overline{F}_{2_i}(t) = \frac{1}{NR}\sum_{w=1}^{NR}\left\|\overline{\boldsymbol{u}}_{t_i}(\boldsymbol{x}_i,t) - \overline{\boldsymbol{u}}_{t_w}(\boldsymbol{x}_i+\boldsymbol{b},t)\right\|_w^2(1+\varepsilon), \tag{7}$$

being $\boldsymbol{u}_t$ is the velocity on the points (due to uniform flow, source panels and vortex cloud), $NR$ the number of rough points and $(1+\varepsilon)$ the kinetic energy gain due to the roughness effects. Bimbato (2012) used 21 rough points on each semicircle defined around each shedding point; this number is enough to obtain a reasonable value for the speeds difference. Equation (6) indicates the relation between the Lamb vortex core and the Reynolds number. If the roughness effects are important ($v_{t_i}(t) \neq 0$), the $k^{th}$ Lamb vortex core must be modified for:

$$\sigma_{0c_k}(t) = 4.48364\sqrt{\frac{\Delta t}{Re}\left(1+\frac{v_{t_i}(t)}{v}\right)}\chi\,, \tag{8}$$

where $\sigma_{0c_k}$ is the core of the $k^{th}$ vortex element positioned at $i^{th}$ shedding point and modified by the roughness model.

According the importance of the local roughness effects, each nascent vortex element can be placed at different positions (from the same pivotal point reference) during each time step of a numerical simulation. The physical sense is that an additional inertial effect is imposed on each nascent vortex element due to the roughness model. This effect changes the strength of the $k^{th}$ vortex element necessary to ensure the no-slip condition.

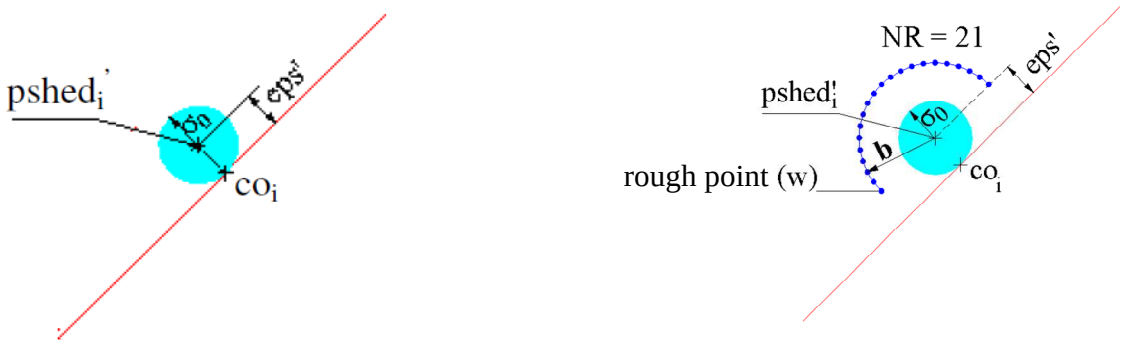


(a) smooth surface (b) rough surface

Figure 2. Vorticity generation process on the Lagrangian Vortex Method (retired of Bimbato et al., 2013).

The present Lagrangian Vortex Method represents the vorticity field by Lamb vortex elements. As was discussed in the final of Section 2 the eddy viscosity is computed to each vortex element during all steps of a typical numerical simulation. In this context, the numerical procedure is conducted over a series of small discrete time steps Δt for each of which a vortex element $\Gamma_k$ is shed from the smooth or rough body surface. The velocity field is calculated at the location of each vortex element (due to the uniform flow, the source panels and the vortex-vortex interaction) in a typical Lagrangian description using an algorithm that splits the advective-diffusive operator of the vorticity transport equation (Chorin, 1973). The vortex-vortex interaction is obtained from the vorticity field by means of the Biot-Savart law. The advective motion of each vortex element generated from the body surface is determined by integration of each vortex path equation using a first order Euler scheme. The viscous diffusion is simulated for each $k^{th}$ vortex element by using a fractional random walk method introduced by Lewis (1999) and modified by Alcântara Pereira et al. (2002) such as:

$$\varsigma_k(t) = \sqrt{\frac{4\Delta t}{Re_{c_k}} ln\left(\frac{1}{P}\right)}\left[cos(2\pi Q)_x + sin(2\pi Q)_y\right], \text{ being } Re_{c_k} = \frac{Ud}{\upsilon + \upsilon_{t_i}(t)} \ , \tag{11}$$

and P e Q random numbers between 0.0 and 1.0. For more details see Bimbato (2012).

The vorticity diffusion takes into account the turbulence modeling. As consequence, the second-order velocity structure function of the filtered field is evaluated for each vortex element through:

$$\overline{F}_{2_j} = \frac{1}{N}\sum_{k=1}^{N}\left\|\overline{\boldsymbol{u}}_{t_j}(\boldsymbol{x}_j) - \overline{\boldsymbol{u}}_{t_k}(\boldsymbol{x}_j + \boldsymbol{r}_k)\right\|_k^2\left(\frac{\sigma_{0_j}}{\boldsymbol{r}_k}\right)^{2/3} \ , \tag{10}$$

where $\overline{\boldsymbol{u}}_t$ represents the total velocity at each the vortex element, $N$ indicates the number of vortex elements inside the circular crown and $\boldsymbol{r}_k$ is the distance between the vortex element under analysis ($j^{th}$ Lamb vortex) and the vortex elements inside the circular crown (each of $k^{th}$ Lamb vortex).

The idea of compute the eddy viscosity no using all vortex elements is to divide the domain in manner that neighborhood of one vortex under analysis is directly taken into account in the Eq. (10). Figure (3) schematically shows the basic idea where, during each time step of simulation, $4^{\ell}$ boxes are constructed to delimit the fluid domain containing vorticity. In this approach $\ell$ defines the box levels. For instance, when $\ell = 1$ the two-dimensional fluid domain is divided in $2^1$ boxes in the x direction and $2^1$ boxes in the y direction.


Figure 3. Examples of boxes structure construction using three levels to compute the eddy viscosity.

The length of each box is given by $\Delta x = L_x / 2^{\ell}$ and $\Delta y = L_y / 2^{\ell}$, where $L_x$ and $L_y$ are the lengths of each side corresponding to the level 0, see Fig. (3). Note that when the level is zero $(i = 1 \text{ and } j = 1)$ is adopted all vortex elements present in the vortex cloud must be considered to compute the eddy viscosity associated to the each vortex element. The level 0 implies a higher computational cost. The localization of each $k^{th}$ vortex element in the fluid domain associated to the corresponding box can be calculated by (being $(x_0, y_0) = (0,0)$):

$$i = \left(\frac{y_k - y_0}{\Delta y}\right) + 1 \ , \tag{12}$$

$$j = \left(\frac{x_k - x_0}{\Delta x}\right) + 1 \ . \tag{13}$$

The present computational strategy only considers the interaction between neighboring boxes, because they would be influencing vortex elements within a distance comparable to that inside the circular crown. Suppose one wishes to calculate the viscosity eddy for all vortex elements located at box 2,3 when level 2 is used (please, see in the Fig. (3)). For this purpose, the eddy viscosity computations are strongly accelerated because only the influence of all vortex elements in the dark grey boxes is computed.

## 4. RESULTS AND CONCLUSIONS

The first providence was to validate the vortex code by simulating the flow around a stationary circular cylinder without turbulence modeling (case I from Tab. 1). The following numerical parameters used here were successfully investigated by Bimbato (2012): number of source flat panels used to represent the cylinder surface ( $NP = 300$ ), time increment ( $\Delta t = 0.05$ ) and the Lamb vortex core ( $\sigma_0 = 0.001d$ ). All the aerodynamic loads computations were evaluated between $8.5 \leq t \leq 45$ . As can be seen in the Table 1, the numerical results for smooth cylinder (case I and case II) agree very well with the experimental ones obtained by Blevins (1984), which have an uncertainty of about ±10%. All numerical results presented in the Tab. (1) used level 0.

Table 1. Time-averaged values of drag and lift coefficients and Strouhal number for circular cylinder ( $Re = 10^5$ )

| Authors | Turbulence Modeling | $\varepsilon/d$ | $\overline{C_D}$ | $\overline{C_L}$ | $\overline{St}$ | $\overline{\theta_{sep}}$ |
|---|---|---|---|---|---|---|
| Blevins (1984) | - | 0.0000 | 1.20 | - | 0.19 | 82° |
| Present result (case I) | No | 0.0000 | 1.25 | 0.00 | 0.200 | 84° |
| Present result (case II) | Yes | 0.0000 | 1.19 | 0.02 | 0.21 | 83° |
| Present result (case III) | Yes | 0.0010 | 1.20 | -0.05 | 0.21 | 86° |

It can be seen from Table 1 that the time-averaged lift coefficient, although very small, is not zero which is due to numerical approximations, and also for a small roughness ( $\varepsilon/d = 0.001$ ) there is just a small perturbation in the boundary layer formed on body surface. Therefore, there is no significant change on aerodynamic forces behavior as reported by Bimbato (2012).

The time-averaged pressure coefficient calculated for the smooth cylinder without turbulence modeling (case I) is shown in the Fig. 4(a). This one is compared with the potential flow pressure distribution and the experimental value presented by Blevins (1984). In the Fig. 4(b) are plotted the aerodynamic forces time history for the same case. One can be observed that the vortex shedding period can be seen in oscillations of the lift and drag coefficients, and also the drag coefficient oscillates two times more than the lift coefficient, which is a characteristic of an isolated circular cylinder. This mechanism of vortex shedding is in agreement to the one proposed by Gerrard (1966); it is repeated periodically causing the oscillating von Kármán street. The frequency of this detachment of vortices is measured by the Strouhal number defined as $St = fd/U$ , being $f$ the detachment frequency of vortical structures (see Tab. 1).

The separation point obtained by the present simulation with turbulence modeling (case II) is about $\theta \cong 83°$ while Blevins (1984) experimentally measured $\theta = 82°$ . Another experimental investigation made by Son and Hanratty (1969) determined a value of $\theta = 78°$ for the separation angle, which agree with experimental results presented by Achenbach (1968). Just before transition into the critical region at $Re = 2.6 \times 10^5$ , the boundary layer is still laminar and separates at an angle $\theta = 94°$ . Hence, separation takes place in the laminar mode as experimentally expected for a subcritical Reynolds number forming free shear layers.

Figure 5 presents the computed values for the drag and lift coefficients of smooth cylinder (case II) and of rough cylinder (case III) with turbulence modeling.

The goal of this work is to show that the algorithm created to compute the eddy viscosity uses less computational effort. For this purpose it was measured the time to compute the coefficient $v_t$ (Eq. 4) for different levels of 25 in 25 time steps using the vortex structures of the case I. Figure 6 shows the comparison of the time spend between each level above referred and the level 0. It is important to emphasize that the mentioned time was computed inside of each time step (such as 1, 26, 51, 76, 101,... 976). According to the Fig. 6(a), the time spend with level 2 is more onerous (for time steps higher than 301), but for the other levels (3, 4, 5 and 6) one can observe larger decrease of time to compute the coefficient $v_t$ . This happen because for higher levels the computational domain with vorticity is divided in more box, therefore, to calculate the eddy viscosity a smaller proportion of this one is verified in order to determinate the influent vortex clusters in the local eddy viscosity computation. Figure 7 shows the position of the vortex wake structure of an isolated circular cylinder at t=48.8 (case I from Tab. 1), when the box structure for level 5 was investigated.

The results from Fig. 6 are summarized in the Tab. 2; it is shown the percent of time spend of each level in relation to the level 0.

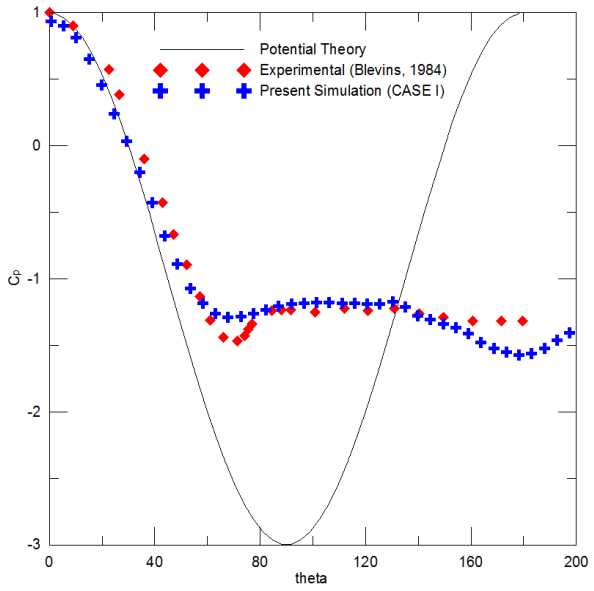


(a) time-averaged pressure coefficient

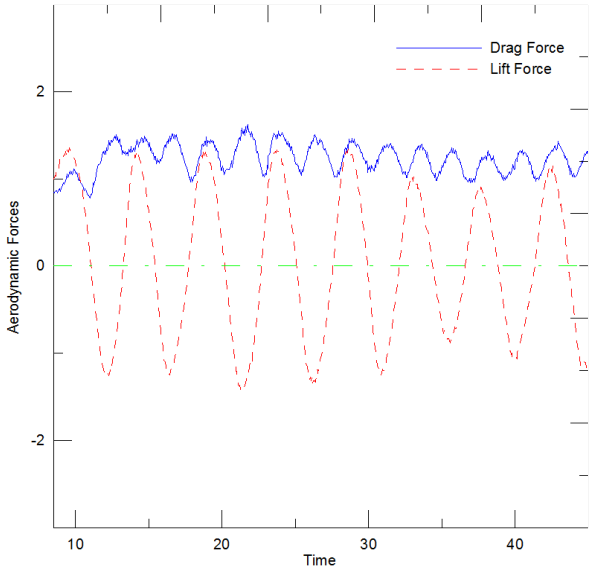


(b) temporal series of drag and lift coefficients

Figure 4. Aerodynamic loads acting on a smooth circular cylinder, case I ( $Re = 10^5$ ).

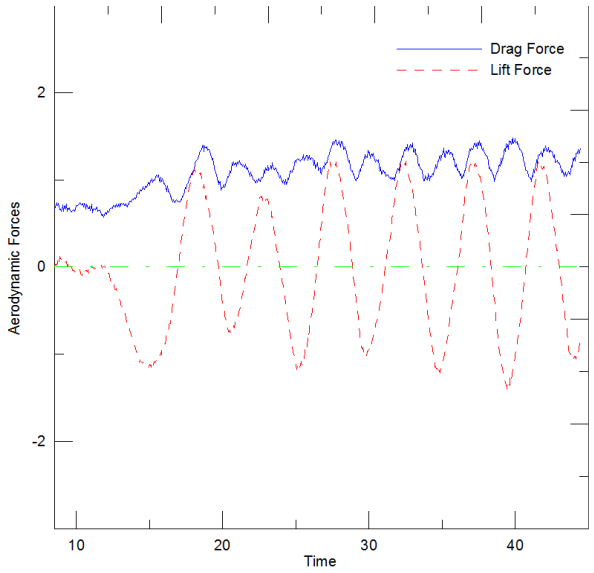


(a) smooth circular cylinder (case II)

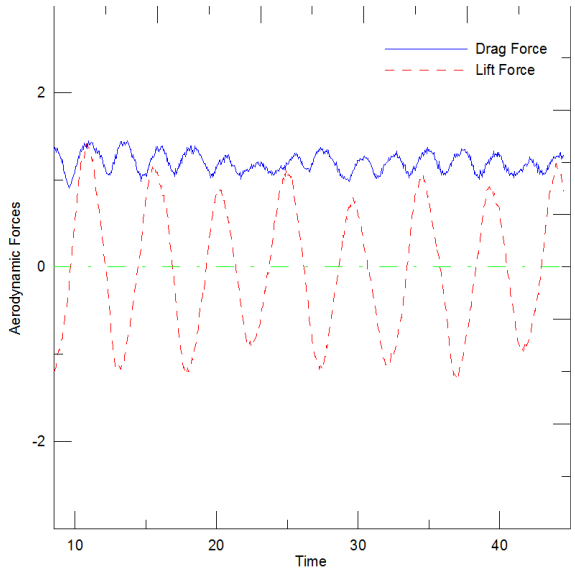


(b) rough circular cylinder (case III)

Figure 5. Aerodynamic loads acting on a circular cylinder with $Re = 10^5$ .

Table 2. CPU times summary necessary to compute $v_t$ using the other levels for comparison with level 0 (case I)

| | Computed time only for step=976 (t=48.8) | Computed accumulated time of 25 in 25 time steps | Comparison of column 2 with time of the level 0 (%) |
|---|---|---|---|
| level 0 | 8.04 min. | 1 hour and 48.71 min. | 100.00 |
| level 2 | 15.21 min. | 3 hours and 4.36 min. | 169.60 |
| level 3 | 5.37 min. | 1 hour and 5.87 min. | 60.59 |
| level 4 | 1.79 min. | 25.33 min. | 23.30 |
| level 5 | 0.73 min. | 10.81 min. | 9.94 |
| level 6 | 0.55 min. | 7.51 min. | 6.91 |

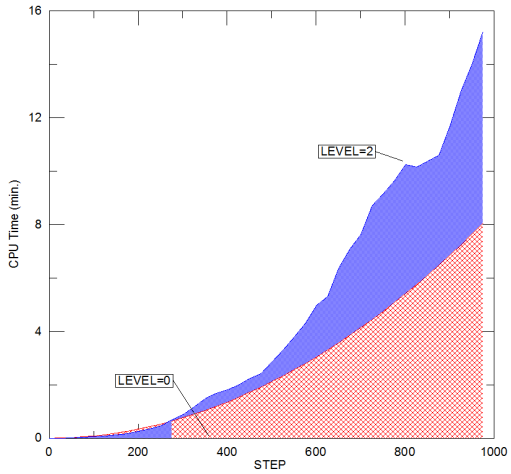


(a) level 0 compared with 2

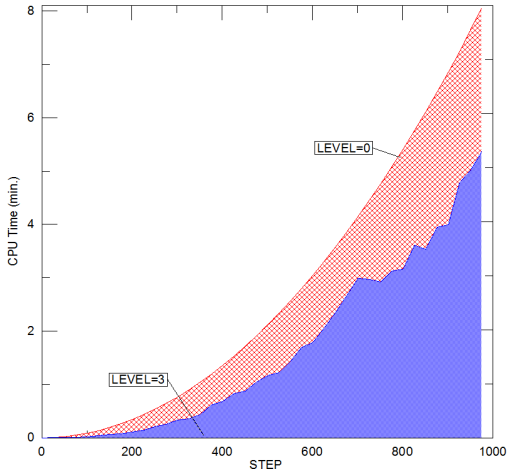


(b) level 0 compared with 3

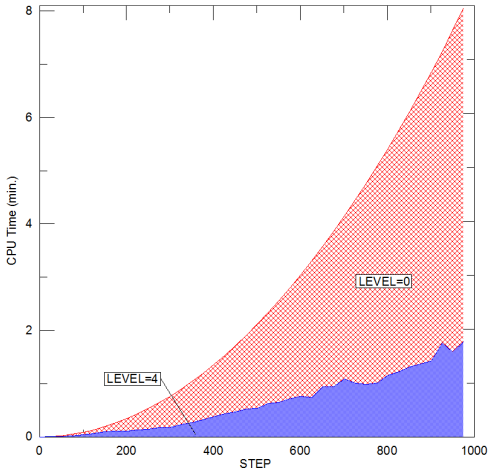


(c) level 0 compared with4

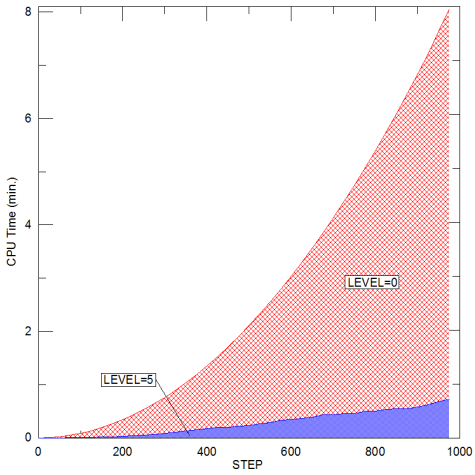


(d) level 0 compared with 5

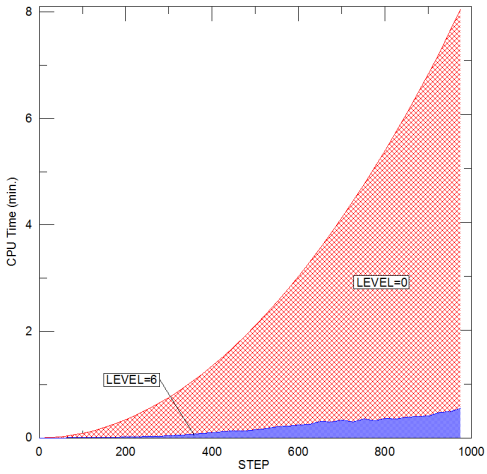


(e) level 0 compared with level 6

Figure 6. CPU times spend to compute the eddy viscosity in different levels (computed of 25 in 25 time steps; case I).

The present results show that the vortex code developed using a Lagrangian Vortex Method with LES modeling is able to solve an unsteady separated flow around a bluff body in a good sense. The time optimization purpose to compute the eddy viscosity is justified since the time spend to simulate the typical flow around an isolated circular cylinder between t=0 and t=48.8 represented 31.14% of time spend in the total simulation (case III as reference).

The first hard computational calculate that spends more CPU time is the Biot-Savart law (exactly 50% of the total time of simulation). Future work will use parallel computation (FORTRAN/LINUX compiler using OpenMP) aiming to reduce the CPU time necessary for this one. It is important to point out that the turbulence computation, how it was calculated initially (level=0), spend over than 30% of the time of all run time. The simulation of case III spent 136 hours in a computer with the follow configuration: INTEL CORE I7 - 2.8GHZ (BOX) 8MB CACHE (i7-860), MB INTEL DH55TC, 8GB RAM DDR3 1333 MHZ. Therefore, the purpose of this paper was succesly achieved.

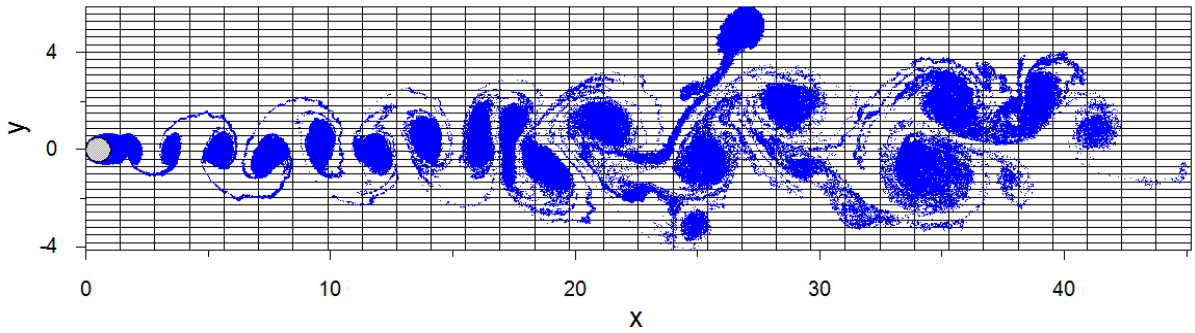


Figure 7. Position of the discrete vortices at $t = 48.00$ for an isolated circular cylinder by using level 5 ( $Re = 10^5$ ).

## 5. ACKNOWLEDGEMENTS

This work was supported by FAPEMIG (Proc. APQ-02175-14) and by Coordination for the Improvement of Higher Education Personnel (CAPES), Proc. PRPPG32003013002D7/UNIFEI.

## 6. REFERENCES

Achenbach, E., 1968, "Distribution of Local Pressure and Skin Friction around a Circular Cylinder in Cross-Flow up to $\mathrm{Re} = 5.0\times10^6$ ", J. Fluid Mech., 34(4): 625-639.

Alcântara Pereira, L. A., Ricci, J. E. R., Hirata, M. H. and Silveira Neto, A., 2002. "Simulation of the Vortex-Shedding Flow about a Circular Cylinder with Turbulence Modeling". *CFD Journal*, Vol. 11, n. 3, pp. 315-322, October.

Bimbato, A. M., Alcântara Pereira, L. A. and Hirata, M. H., 2013. "Numerical Investigation of the Drag Crisis in Flow Past a Rough Circular Cylinder". In Proceedings of the COBEM 2013 22nd International Congress of Mechanical Engineering. Ribeirão Preto, SP, Brazil.

Bimbato, A. M., 2012. "Study of Turbulent Flows around a Smooth or a Rough Bluff Body Using the Discrete Vortex Method". D.Sc. Thesis, Institute of Mechanical Engineering, UNIFEI, Itajubá, MG, Brazil (in Portuguese).

Chorin, A. J., 1973. "Numerical Study of Slightly Viscous Flow". *Journal of Fluid Mechanics*, Vol. 57, pp. 785-796.

Gerrard, J.H., 1966, "The Mechanics of the Formation Region of Vortices behind Bluff Bodies", J. Fluid Mech., 25: 401-413.

Guven, O., Farell, C. and Patel, V. C., 1980. "Surface Roughness Effects on the Mean Flow past Circular Cylinders". Journal of Fluid Mechanics, Vol. 98, pp. 673-701.

Katz, J. and Plotkin, A., 1991. "Low Speed Aerodynamics: From Wing Theory to Panel Methods". McGraw Hill, Inc.

Kamemoto, K., 2004, "On Contribution of Advanced Vortex Element Methods Toward Virtual Reality of Unsteady Vortical Flows in the New Generation of CFD", Proceedings of the 10th Brazilian Congress of Thermal Sciences and Engineering-ENCIT 2004, Rio de Janeiro, Brazil, Nov. 29 - Dec. 03, Invited Lecture-CIT04-IL04.

Kundu, P. K., 1990. "Fluid Mechanics". Academic Press.

Lewis, R.I., 1999, "Vortex Element Methods, the Most Natural Approach to Flow Simulation - A Review of Methodology with Applications", Proceedings of 1st Int. Conference on Vortex Methods, Kobe, Nov. 4-5, pp. 1-15.

Shintani, M., Akamatsu, T., 1994. "Investigation of Two-Dimensional Discrete Vortex Method with Viscous Diffusion Model". CFD Journal, vol. 3, n. 2, pp. 237-254.

Smagorinsky, J., 1963. "General Circulation Experiments with the Primitive Equations". Mon. Weather Rev., Vol. 91, n. 3, pp. 99-164.

Son, J.S. and Hanratty, T.J., 1969, "Velocity Gradients at the Wall for Flow around a Cylinder at Reynolds Number from $5{,}0\times10^3$ to $1{,}0\times10^5$ ", J. Fluid Mech., 35 (2): 353-368.

## 7. RESPONSIBILITY NOTICE

The authors are the only responsible for the printed material included in this paper.